ResearchGate

See discussions, stats, and author profiles for this publication at: https://www.researchgate.net/publication/257619925

Pore System Characterization and Petrophysical Rock Classification Using a Bimodal Gaussian Density Function

Article *in* Mathematical Geosciences · August 2013

DOI: 10.1007/s11004-013-9473-2

CITATIONS
74

READS
866

2 authors, including:

Chicheng Xu
Aramco Houston Research Center
35 PUBLICATIONS **476** CITATIONS

SEE PROFILE

All content following this page was uploaded by Chicheng Xu on 30 August 2019.

The user has requested enhancement of the downloaded file.

Math Geosci
DOI 10.1007/s11004-013-9473-2

Pore System Characterization and Petrophysical Rock Classification Using a Bimodal Gaussian Density Function

Chicheng Xu · Carlos Torres-Verdín

Received: 2 February 2013 / Accepted: 21 May 2013
© International Association for Mathematical Geosciences 2013

Abstract This paper introduces a bimodal Gaussian density function to characterize pore-size distributions in terms of incremental pore volume versus logarithmic pore-throat radius. An inverse problem is formulated and solved to reconstruct mercury injection capillary pressure curves by enforcing a bimodal Gaussian pore-size distribution. The bimodal Gaussian model generates six petrophysically interpretable attributes which provide a quantitative basis for petrophysical modeling and rock typing. Correlations between these attributes and their associated petrophysical properties are investigated to verify interpretations. In the field case, the correlation coefficient (R^2) between absolute permeability, end-point gas relative permeability and the mean value of large pore-throat size mode are 0.93 and 0.715, respectively. Correlation ($R^2 = 0.613$) is also observed between critical water saturation and pore volume connected by small pore-throat sizes. Petrophysical modeling based on the bimodal Gaussian pore-size distribution with sufficient core data calibration predicts static and dynamic petrophysical properties that are in agreement with laboratory core measurements. The quantitative pore-system description underlies a new petrophysical rock typing method that combines all relevant pore-system attributes. Verification of the method was performed with field data from two key wells in the Hugoton carbonate gas field, Kansas.

Keywords Bimodal Gaussian density function · Inverse problem · Pore-size distribution · Petrophysical modeling · Rock typing

C. Xu (✉) · C. Torres-Verdín
Petroleum & Geosystems Engineering Department, The University of Texas at Austin,
200 E. Dean Keeton St., Stop C0300, Austin, TX 78712-1585, USA
e-mail: xuchicheng@mail.utexas.edu

C. Torres-Verdín
e-mail: cverdin@mail.utexas.edu

Published online: 30 July 2013

1 Introduction

Pore-size distribution relates all petrophysical properties, which is the central theme in petrophysical characterization of reservoir rocks (Archie 1950). Different forms of pore-size distribution from various data sources have been documented and compared in the existing technical literature (Basan et al. 1997). In this paper, pore-size distribution refers to incremental pore volume versus logarithmic pore-throat radius (denoted as $\log R$), which can be derived from mercury injection capillary pressure (MICP) curves (Peters 2012). Several types of density functions have been used to model pore-size distributions or related petrophysical measurements analytically. The first type of density function is that of Thomeer (1960), who invoked hyperbolic functions to fit MICP curves. This procedure implicitly makes use of the derivative of Thomeer's hyperbolas (referred to as Thomeer's derivative) as the pore-size distribution function. Several authors (Clerke 2009; Gao et al. 2011) reported the use of multiple Thomeer's hyperbolas to characterize complex carbonate rock pore systems. The use of Thomeer's parameters for saturation-height modeling, upscaling, and rock typing have been reported elsewhere (Thomeer 1960; Clerke et al. 2008; Buiting 2011). In addition, Hidajat et al. (2004) used a trimodal Weibull distribution to fit nuclear magnetic resonance (NMR) T_2 spectra, which is closely correlated to the pore-body size distribution when the rock is fully water saturated. Similarly, Genty et al. (2007) fitted NMR T_2 spectra using up to three Gaussian components. In fact, Gaussian (or log-normal) density functions have been routinely used for modeling pore-size and grain-size distributions in the open technical literature (Spencer 1963; Nimmo 2004). The parameters associated with a Gaussian density function relate directly and intuitively to pore-system attributes. However, only a relatively small body of work has been documented on the interpretation and petrophysical meaning of these Gaussian attributes and on their use for petrophysical modeling and rock classification.

In this paper, an inverse problem is formulated to fit MICP curves based on a bimodal Gaussian pore-size distribution model. A set of six attributes included with each bimodal Gaussian density function is estimated and interpreted for petrophysical meaning and subsequently used in petrophysical modeling to predict rock petrophysical properties. Results from fitting MICP data from two key wells in the Hugoton carbonate gas field confirm that bimodal Gaussian density functions are appropriate to describe complex pore systems. A new petrophysical rock typing method that combines all Gaussian attributes is introduced after fitting MICP data, which provides better ranking of rock types and shows petrophysical consistency among all static and dynamic properties. The main advantage of this new rock typing method is that it simultaneously considers pore volume, pore connectivity, and pore-size uniformity as input attributes for petrophysical classification, while existing core-based petrophysical rock typing methods tend to rely dominantly on hydraulic radius to rank reservoir rocks (Xu and Torres-Verdín 2012).

2 Pore-System Characterization with a Bimodal Gaussian Density Function

Pore-throat size is empirically characterized on a logarithmic scale due to its large variability across several orders of magnitude. Therefore, all Gaussian density func-

tions in this paper treat the distribution of pore-throat size on a logarithmic scale (i.e., log-normal distribution).

2.1 Bimodal Gaussian Pore-Size Distribution

A bimodal Gaussian density function is expressed as

$$p(\log R; w_1, \log \mu_1, \log \sigma_1; w_2, \log \mu_2, \log \sigma_2) = w_1 \frac{1}{\sqrt{2\pi}\log \sigma_1} e^{-\frac{(\log R - \log \mu_1)^2}{2(\log \sigma_1)^2}} + w_2 \frac{1}{\sqrt{2\pi}\log \sigma_2} e^{-\frac{(\log R - \log \mu_2)^2}{2(\log \sigma_2)^2}}, \quad (1)$$

where R is pore-throat radius in μm, w_1 and w_2 are weighting coefficients for each Gaussian mode, $\log \mu_1$ and $\log \mu_2$ are the mean values of logarithmic pore-throat radius, and $\log \sigma_1$ and $\log \sigma_2$ are the corresponding standard deviations of logarithmic pore-throat radius. The following constraints apply to the Gaussian attributes included in Eq. (1):

$$w_1 + w_2 = 1.0, \quad \text{and} \quad 0 < w_{1,2} < 1.0. \quad (2)$$

The corresponding cumulative distribution function (CDF) is given by

$$P(\log R; w_1, \log \mu_1, \log \sigma_1; w_2, \log \mu_2, \log \sigma_2) = \frac{w_1}{2}\left[1 + \text{erf}\left(\frac{\log R - \log \mu_1}{\sqrt{2(\log \sigma_1)^2}}\right)\right] + \frac{w_2}{2}\left[1 + \text{erf}\left(\frac{\log R - \log \mu_2}{\sqrt{2(\log \sigma_2)^2}}\right)\right] \quad (3)$$

where erf function is the Gaussian error function, given by

$$\text{erf}(z) = \frac{2}{\sqrt{\pi}} \int_0^z e^{-t^2}\, dt. \quad (4)$$

Figure 1 shows a typical bimodal Gaussian density function and its corresponding CDF. Overlapping of two independent Gaussian modes of pore-size distribution is commonly observed with experimental data.

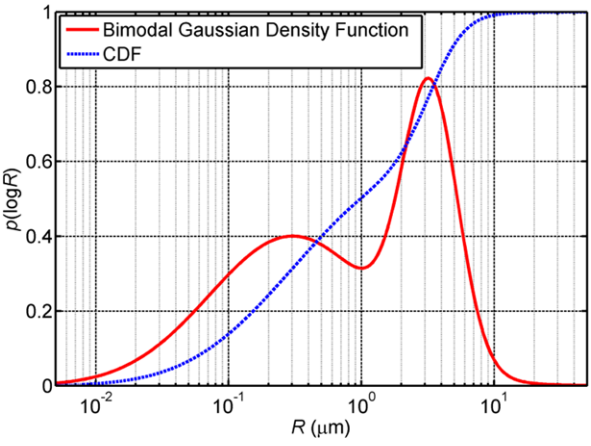

Fig. 1 Example of a bimodal Gaussian density function and corresponding CDF

2.2 Petrophysical Interpretation of Gaussian Attributes and CDF

As emphasized by Eq. (1), a bimodal Gaussian density function includes six attributes to describe a pore-size distribution. Each attribute has petrophysical implications interpreted as follows:

w_1: fraction of pore volume connected by large pore-throat sizes where most residual non-wetting phase preferentially resides during imbibition (Handy and Datta 1966; Mohanty and Salter 1982). Flow capacity or permeability of reservoir rocks is dominantly controlled by this fraction of pore volume and the associated pore-throat radius (μ_1).

w_2: fraction of pore volume connected by small pore-throat sizes where most irreducible wetting phase preferentially resides during drainage; therefore, its contribution to fluid flow is marginal.

$\log \mu_1$ and $\log \mu_2$: mean values of large and small logarithmic pore-throat radius modes, respectively; larger values indicate larger fluid-flow conduits as well as higher hydraulic conductivity; μ_1 is correlated with hydraulic radius.

$\log \sigma_1$ and $\log \sigma_2$: standard deviation of large and small pore-throat radius modes, which represents the uniformity of "capillary tube sizes" (Childs and Collis-George 1950); a larger value indicates lower sorting of tube sizes and higher tortuosity of the pore network, thereby lower permeability given the same mean value of pore-throat radius and pore volume.

CDF: capillary pressure in the "bundle-of-capillary-tubes" model, according to Laplace's equation, given by

$$P_c = \frac{2\Gamma|\cos\theta|}{R}, \tag{5}$$

where R is pore-throat radius in μm, Γ is interfacial tension, and θ is contact angle. For the CDF shown in Fig. 1, pore-throat radius on the x axis can be transformed to capillary pressure using Eq. (5), whereas the y axis is equivalent to wetting-phase saturation. Therefore, the CDF is equivalent to a standard capillary pressure curve.

3 Derivation of the Bimodal Gaussian Pore-Size Distribution from MICP Data

Two methods are used to estimate a bimodal Gaussian pore-size distribution from MICP data. The first (or differentiation) method derives a pore-size distribution by differentiating S_w (wetting-phase saturation) with respect to $\log R$ from MICP data and then decomposes the distribution into two Gaussian components using a Gaussian mixture model algorithm (Press et al. 2007). The second (or inversion) method solves an inverse problem to estimate a bimodal Gaussian pore-size distribution by minimizing the quadratic residual between the modeled S_w and the measured S_w at all lab-used capillary pressure points (see Appendix A for details of the formulation). In practice, it is often difficult to obtain a smooth pore-size distribution from the differentiation method due to both limited number of measurement points and noisy data. Therefore, the inversion method is preferred in this paper to provide stable and

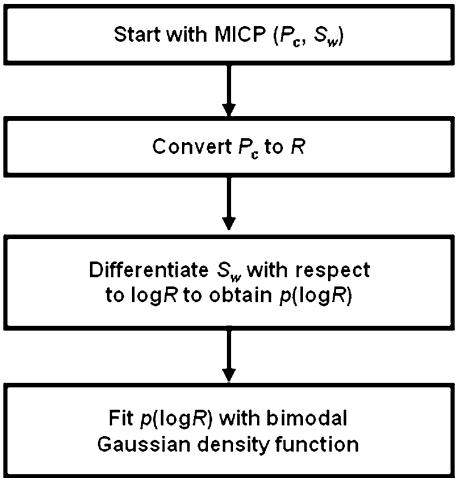

Fig. 2 Workflow used to derive a bimodal Gaussian pore-size distribution by differentiating S_w with respect to log$R$ and then fitting the results with a Gaussian mixture model

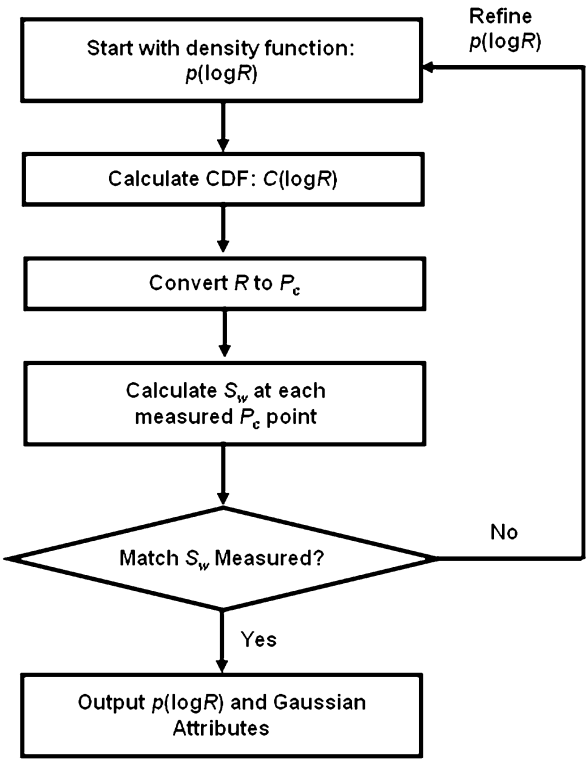

Fig. 3 Workflow used to derive a bimodal Gaussian pore-size distribution by iteratively matching MICP data using inversion

smooth results. Figures 2 and 3 show the workflows of the differentiation and inversion methods, respectively. Figures 4 and 5 compare results obtained when applying the two methods to an example of MICP data from the Hugoton gas field.

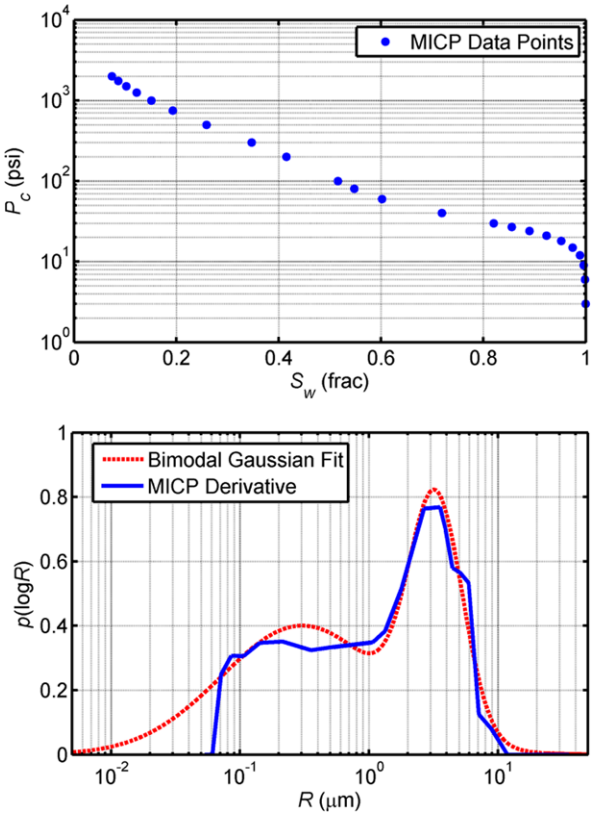

Fig. 4 Example of derivation of a bimodal Gaussian pore-size distribution from MICP data using the differentiation method. Differentiation of experimental data is commonly noisy (Peters, 2012)

4 Field Case: The Hugoton Gas Field, Kansas

The Hugoton field in Kansas is one of the largest conventional gas fields in North America. It has cumulatively produced more than 23 trillion cubic feet of gas during the past 70 years (Olson et al. 1997). Gas production originates mainly from the Lower Permian Chase and Council Grove Groups. The reservoir is divided into 13 stratigraphic intervals that have complex lithofacies spreading from continental and marine siltstones to sandstones, mudstone to grainstone limestones, fine- to medium-crystalline dolomites, and phylloid algal bafflestones (Dubois et al. 2006). Consequently, existing rock pore systems are extremely complex due to both depositional control and diagenetic overprints.

Routine core porosity and permeability measurements were acquired from more than 200 core samples (Fig. 6) in two key wells (API No. 15-189-20657 and 15-055-21045). In addition, MICP curves measured from 33 core samples were available for this study (Fig. 7a), among which 13 core samples included measured primary drainage relative permeability curves (Fig. 7b). Core data exhibit large variability in all petrophysical properties, which renders the petrophysical modeling and rock typing work very difficult (Xu et al. 2012). Pore-size distributions are first modeled with bimodal Gaussian density functions for all core-measured MICP curves. The correlation between petrophysical properties (permeability, irreducible water saturation, and

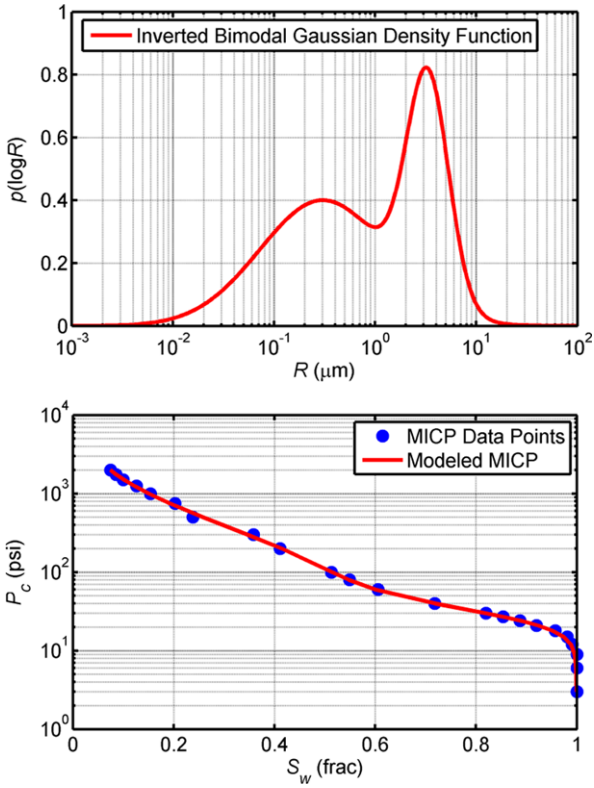

Fig. 5 Example of the derivation of a bimodal Gaussian pore-size distribution from MICP using the inversion method

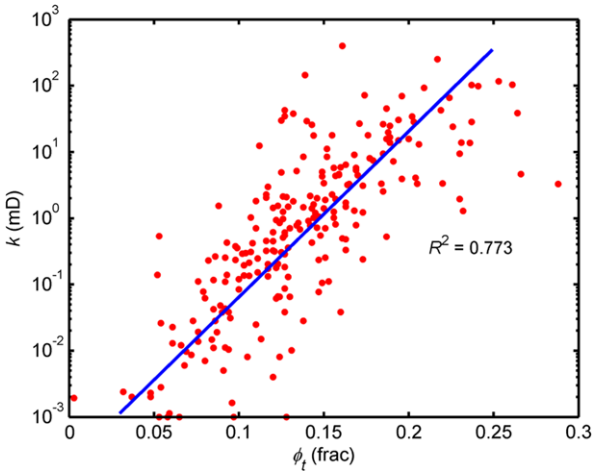

Fig. 6 Crossplot of total porosity and permeability. Large uncertainty is associated with permeability modeling based on porosity-permeability correlation

relative permeability end points) and Gaussian attributes set is then studied to verify the petrophysical interpretation. Based on these Gaussian attributes, a new petrophysical rock typing method is proposed to classify complex carbonate rocks for reservoir characterization studies.

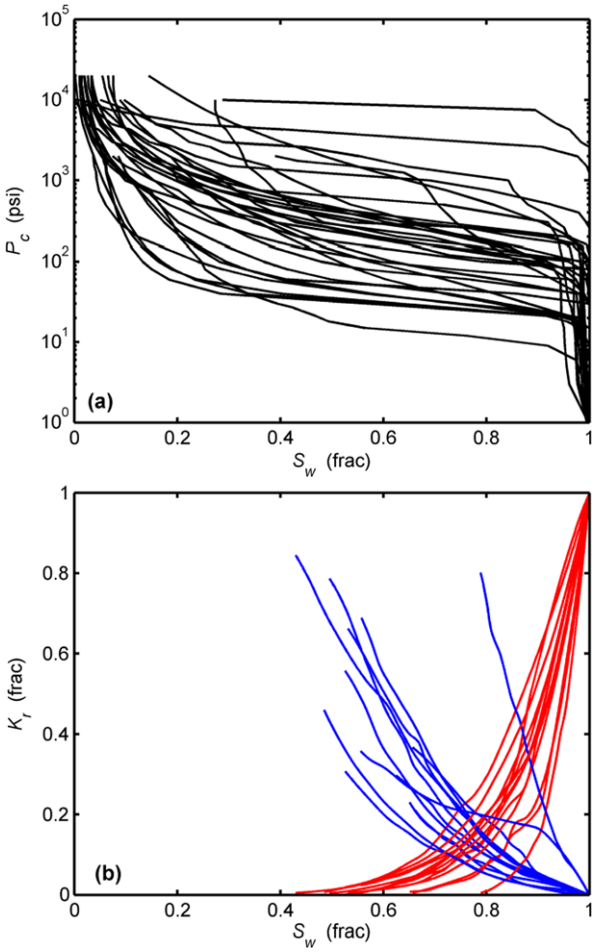

Fig. 7 (**a**) Unclassified MICP capillary pressure curves from 33 core samples, and (**b**) primary drainage relative permeability ($S_{gr} = 0$) curves from 13 core samples acquired in the Hugoton gas field

4.1 Pore-Size Distribution Modeling

The inversion method was applied to derive bimodal Gaussian pore-size distributions from 33 MICP curves. Appendix B summarizes the corresponding results. Histograms of the six Gaussian attributes (Fig. 8) indicate that rocks exhibit wide variability in all petrophysical properties. It is observed that the standard deviation of the large pore-throat size mode is much smaller than those of the small pore-throat size mode, thereby suggesting that most rocks in this study have a narrowly distributed dominant pore-throat radius.

4.2 Absolute Permeability Prediction (k)

Absolute permeability is mainly controlled by the large pore-throat size mode. Figure 9 shows the correlations between permeability and attributes of the large pore-throat size mode. Positive correlation with permeability is observed for the pore volume (Fig. 9a) and the mean pore-throat size (Fig. 9b), whereas correlation between

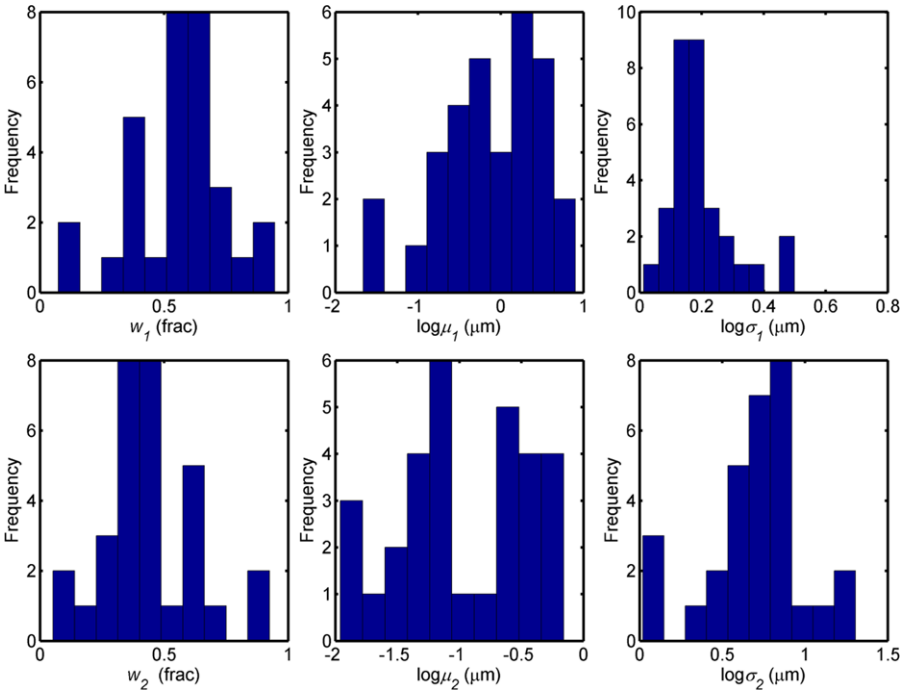

Fig. 8 Histograms of all Gaussian attributes. *Upper* and *lower panels* show the histograms for large and small pore-throat size modes, respectively

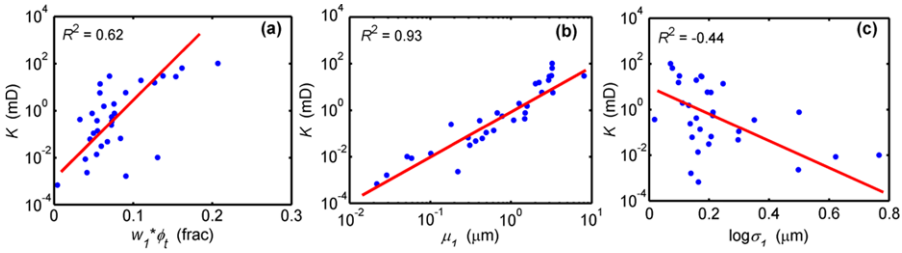

Fig. 9 Correlation between permeability and Gaussian attributes for the large pore-throat size mode: (**a**) pore volume, (**b**) mean value, and (**c**) standard deviation

permeability and standard deviation is negative (Fig. 9c). The highest correlation is observed between permeability and mean value of large pore-throat size mode, with the correlation coefficient (0.93) being much higher than between total porosity and permeability (0.77, as in Fig. 6), thereby suggesting reliability for predicting permeability once μ_1 is known.

4.3 Irreducible Water Saturation (S_{wirr}) and Critical Water Saturation (S_{wcrit})

In a water-wet rock, water preferentially resides in pores connected by the smallest pore throats during migration or drainage. Consequently, irreducible and critical

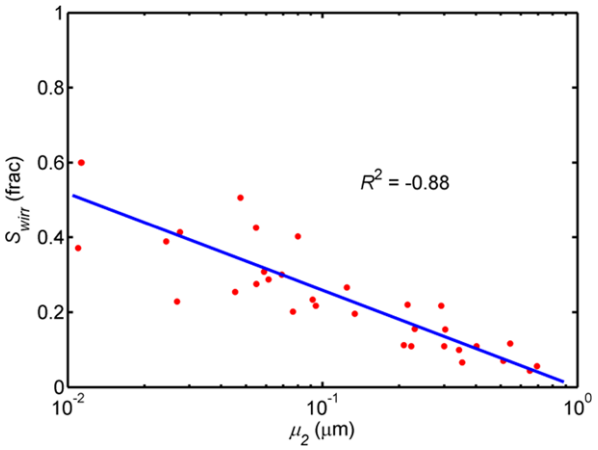

Fig. 10 Correlation between irreducible water saturation (derived from MICP with cutoff $P_c = 1000$ psi) and mean value of the small pore-throat size mode

water saturations are chiefly conditioned by the small pore-throat size mode. Below, we define irreducible and critical water saturations and study their correlations with Gaussian attributes separately.

Irreducible Water Saturation from Capillary Pressure Water saturation that cannot be forced out of the pore system at a given threshold capillary pressure during drainage (10^3 psi in this study). This value is normally used to calculate total hydrocarbon volume in static reservoir modeling. Under such a definition, irreducible water has a high correlation with the mean value of the small pore-throat size mode (Fig. 10, $R^2 = -0.88$).

Critical Water Saturation from Relative Permeability Water saturation (Marschall et al. 1995) at which the corresponding water phase relative permeability is below a threshold value (10^{-4} frac in this study). The latter value is normally larger than irreducible water saturation derived from MICP. It is used to calculate water production in dynamic reservoir modeling. Under this definition, critical water saturation approximates the pore volume fraction associated with the small pore-throat size mode (Fig. 11, $R^2 = 0.613$).

4.4 Gas Relative Permeability End Point (k_{rg} at S_{wirr})

In a water-wet rock, gas is the non-wetting phase that preferentially resides in pores connected by large pore throats while irreducible water remains in the smallest pores. Consequently, permeability to gas is mainly controlled by the large pore throats. Figure 12 shows the correlation between gas relative permeability at critical water saturation and the mean value of large pore-throat size mode (μ_1). The correlation coefficient is 0.715, which ensures a good prediction of the end-point value of gas relative permeability in this particular reservoir when μ_1 is known.

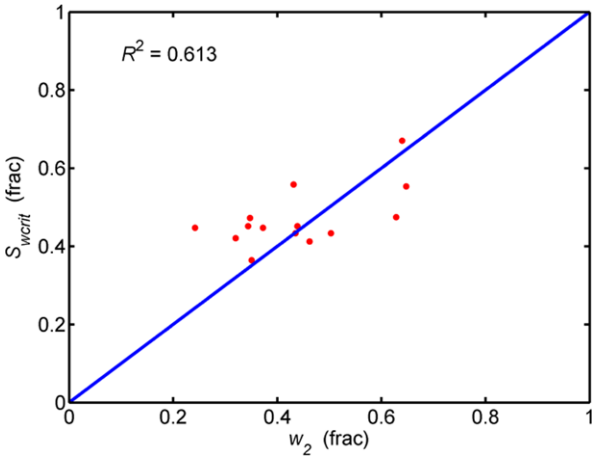

Fig. 11 Correlation between critical water saturation derived from relative permeability and pore volume fraction of the small pore-throat size mode. The blue line identifies the $y = x$ line

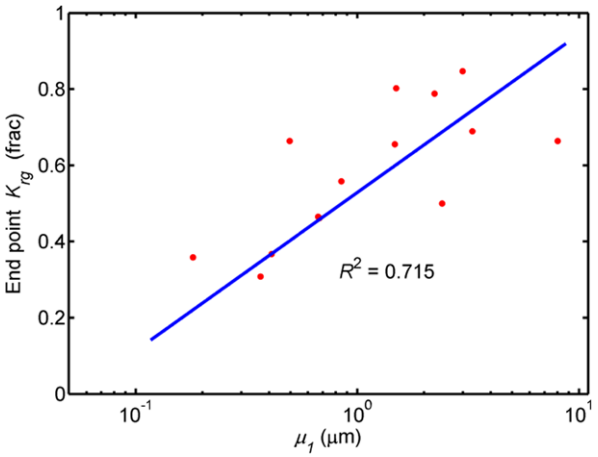

Fig. 12 Correlation between the end-point value of gas relative permeability at critical water saturation and mean value of the large pore-throat size mode

4.5 Residual Gas Saturation (S_{gr}) and End Point Water Relative Permeability (k_{rw} at S_{gr})

Because imbibition capillary pressure and relative permeability were not measured, residual gas saturation is unavailable in this study. Only some theoretical discussions are included to explain the possible relation between Gaussian attributes and residual gas saturation. In a water-wet rock, gas is the non-wetting phase that first invades pores connected by large pore throats during migration or drainage. Consequently, residual gas saturation is mainly determined by the attributes of the large pore-throat size mode when an imbibition cycle begins. Rocks of larger pore-throat radius (larger μ_1) tend to exhibit less gas saturation trapped in the pore system. Given the same mean value of pore-throat radius, rocks of more uniform pore-size distribution (smaller σ_1) tend to exhibit less trapped gas (Mohanty and Salter 1982). However, it is difficult to establish an analytical function between residual gas saturation

and Gaussian attributes. An empirical model may be reliable with sufficient core calibration.

4.6 Modeling Drainage Relative Permeability from MICP Curves

With all previous correlations established, one can derive primary drainage relative permeability curves from the bimodal Gaussian pore-size distribution using Corey–Burdine's model (Burdine 1953; Huang et al. 1997). Critical water saturation (S_{wcrit}) is calculated from its correlation with parameter w_2 (Fig. 11), whereas the end point of gas relative permeability is predicted by its correlation with parameter μ_1 (Fig. 12). The end point of water relative permeability is set to 1.0 and residual gas saturation (S_{gr}) is set to 0 in a primary drainage process. Burdine's wetting-phase relative permeability is given by

$$k_{\text{rw}} = \left(S_w^*\right)^2 \frac{\int_0^{S_w^*} \frac{1}{(P_c)^2}\, dS_w^*}{\int_0^1 \frac{1}{(P_c)^2}\, dS_w^*} = \left(S_w^*\right)^2 \frac{\int_0^{S_w^*} R^2\, dS_w^*}{\int_0^1 R^2\, dS_w^*}, \tag{6}$$

and non-wetting-phase relative permeability by

$$k_{\text{rnw}} = \left(1 - S_w^*\right)^2 \frac{\int_{S_w^*}^1 \frac{1}{(P_c)^2}\, dS_w^*}{\int_0^1 \frac{1}{(P_c)^2}\, dS_w^*} = \left(1 - S_w^*\right)^2 \frac{\int_{S_w^*}^1 R^2\, dS_w^*}{\int_0^1 R^2\, dS_w^*}, \tag{7}$$

where P_c is capillary pressure and R is the corresponding pore-throat radius as in Eq. (5); S_w^* is normalized water saturation, defined as

$$S_w^* = \frac{S_w - S_{\text{wirr}}}{1 - S_{\text{wirr}} - S_{\text{gr}}}. \tag{8}$$

Based on MICP-derived bimodal Gaussian pore-size distribution, primary drainage relative permeability curves modeled with Burdine's equations agree well with core data (Fig. 13).

4.7 Petrophysical Rock Typing

The above Gaussian attributes contain rich petrophysical information, whereby they become suitable for petrophysical rock classification. Multi-dimensional k-means clustering analysis (Press et al. 2007) was performed on the six Gaussian attributes and classified the 33 samples into four rock types. Figure 14a shows that rock types rank well in the porosity and permeability crossplot, with their MICP data also consistently classified by rock type (Fig. 14b). With the same rock type information, the 13 primary drainage relative permeability curves are plotted in Fig. 15. For rock types I, II, and III, reservoir quality decreases as rock type number increases. Accordingly, critical water saturation increases and, on average, the end-point value of gas relative permeability decreases. Rock type IV is mostly non-reservoir rock that acts as baffle or seal in a reservoir. The only relative permeability curve available for this rock type

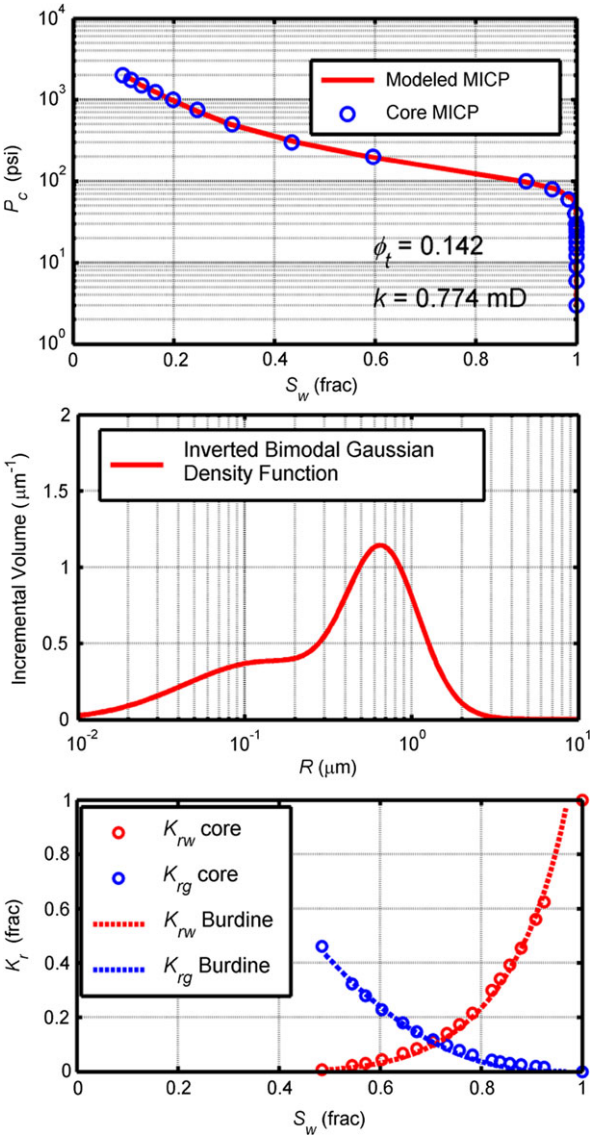

Fig. 13 Modeled primary drainage capillary pressure curves from the bimodal Gaussian pore-size distribution data using Corey–Burdine's model. The end point of water relative permeability is set to 1.0 and residual gas saturation (S_{gr}) is set to 0

(Fig. 15d) is from a special trimodal-pore-sized rock, which has a similar large pore-throat size mode as rock type II and a similar small pore-throat size mode as rock type IV. Consequently, this rock sample exhibits some flow capacity, but it lacks significant initial gas saturation under reservoir capillary pressure conditions. Because of the above results, we did not construct a separate rock type for this particular sample, but still classified it as rock type IV.

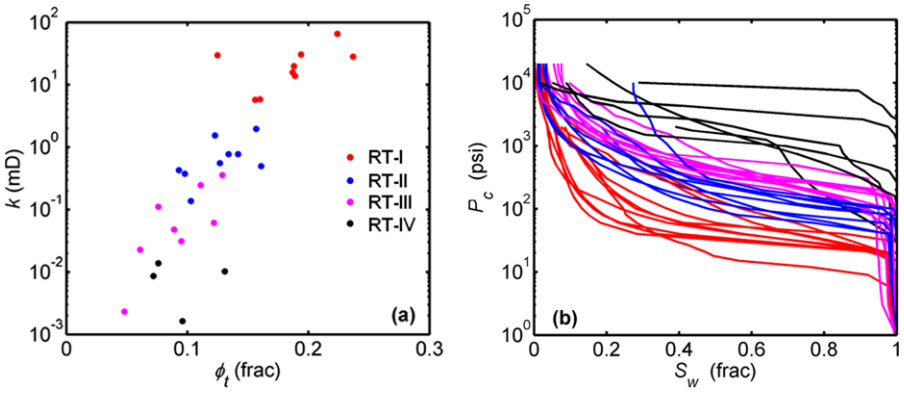

Fig. 14 (**a**) Porosity-permeability crossplot ranked with rock types, and (**b**) MICP data ranked with rock types

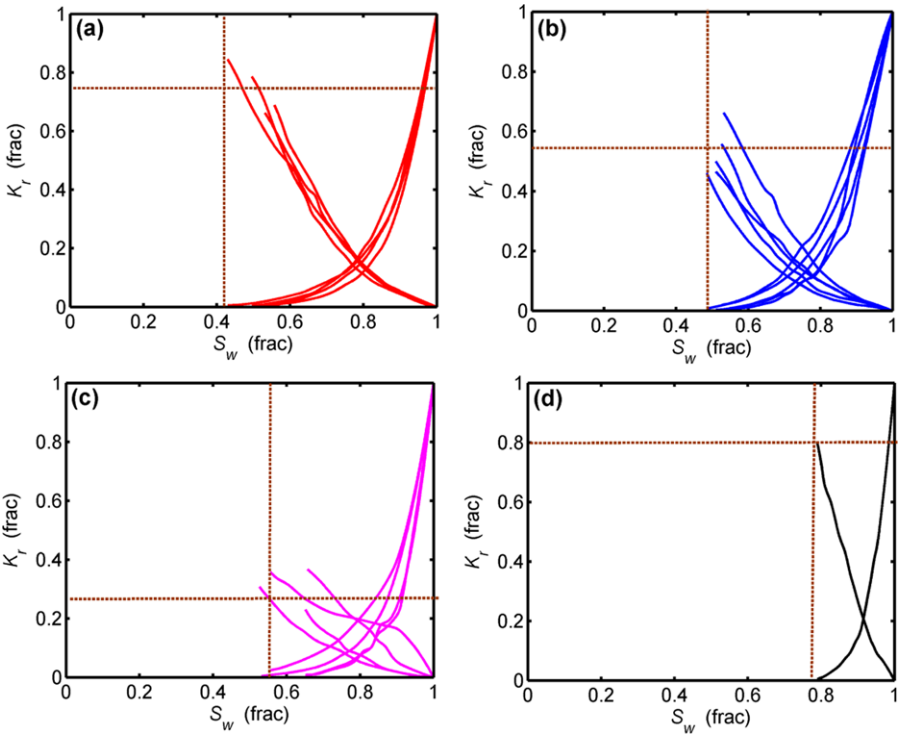

Fig. 15 Primary drainage relative permeability ($S_{gr} = 0$) curves grouped according to rock type: (**a**) rock type I, (**b**) rock type II, (**c**) rock type III, and (**d**) rock type IV

5 Conclusions

Bimodal Gaussian density function is a useful analytical tool to describe complex pore systems. Gaussian attributes included in this model have interpretable petrophysical meaning, which can be quantitatively used for petrophysical modeling and rock typing. Verification studies in the Hugoton gas field yielded the following petrophysical interpretations:

(1) Absolute permeability is mainly controlled by the large pore-throat size mode. It is positively correlated with mean pore-throat radius and the associated pore volume while negatively correlated with standard deviation.
(2) Irreducible or critical water saturation is mainly controlled by the small pore-throat size mode. Both are correlated with the mean value of small pore-throat size mode and the associated pore volume fraction.
(3) The end-point value for gas relative permeability at critical water saturation is mainly controlled by the large pore-throat size mode, especially the mean value.

Moderate to high correlations were observed between Gaussian attributes and various petrophysical properties. Therefore, it is possible to model several static and dynamic petrophysical properties (irreducible and critical water saturation, absolute permeability, drainage relative permeability) based on a bimodal Gaussian density function. Given sufficient core calibration, pore systems in reservoir rocks can be fully characterized by a set of six Gaussian attributes that predict consistent petrophysical properties for subsequent reservoir characterization studies. Petrophysical rock typing based on Gaussian attributes provides reliable ranking of reservoir quality and simplifies reservoir modeling by enforcing a consistent petrophysical description based on pore geometry. However, the classification method proposed in this paper still considers the six Gaussian attributes as individual input. More advanced classification methods that integrate all six Gaussian attributes to define petrophysical dissimilarity are necessary for future implementation.

6 List of Symbols

C	Quadratic cost function, []
k	Absolute permeability, [mD]
K_{rg}	Gas relative permeability, [frac]
K_{rw}	Water relative permeability, [frac]
p	Density function of logarithmic pore-throat radius
P	Cumulative distribution function of logarithmic pore-throat radius
P_c	Capillary pressure, [psi]
R	Pore-throat radius, [μm]
R^2	Correlation coefficient, []
S_{gr}	Residual gas saturation, [frac]
S_w	Wetting Phase or Water saturation, [frac]
S_w^*	Normalized water saturation, [frac]
S_{wcrit}	Critical water saturation, [frac]

S_{wirr}	Irreducible water saturation, [frac]
T_2	NMR transverse relaxation time, [ms]
w_1	Fraction of pore volume connected by large pore-throat size, [frac]
w_2	Fraction of pore volume connected by small pore-throat size, [frac]
W_s	Weighting matrix, []
x	Gaussian attributes vector, []
α	Regularization parameter, []
θ	Contact angle between wetting and non-wetting phase, [degree]
$\log \mu_1$	Mean value of the large pore-throat radius Gaussian mode, [μm]
$\log \mu_2$	Mean value of the small pore-throat radius Gaussian mode, [μm]
Γ	Interfacial tension between wetting and non-wetting phase, [dyne/cm]
$\log \sigma_1$	Standard deviation of the large pore-throat radius Gaussian mode, [μm]
$\log \sigma_2$	Standard deviation of the small pore-throat radius Gaussian mode, [μm]
ϕ_t	Total porosity, [frac]

7 List of Acronyms

API	American Petroleum Institute
CDF	Cumulative Distribution Function
ERF	Gaussian Error Function
MICP	Mercury Injection Capillary Pressure
NMR	Nuclear Magnetic Resonance

Acknowledgements We would like to thank Amoco (now BP), Anadarko, and Mobil (now ExxonMobil) for making their core data acquired in the Hugoton field available to the public. A note of special gratitude goes to the KGS Hugoton Asset Management Project staff for maintaining the database and for sharing their comprehensive reservoir study documents. The work reported in this paper was funded by The University of Texas at Austin's Research Consortium on Formation Evaluation, jointly sponsored by Afren, Anadarko, Apache, Aramco, Baker-Hughes, BG, BHP Billiton, BP, Chevron, China Oilfield Services, LTD., ConocoPhillips, ENI, ExxonMobil, Halliburton, Hess, Maersk, Marathon Oil Corporation, Mexican Institute for Petroleum, Nexen, ONGC, OXY, Petrobras, Repsol, RWE, Schlumberger, Shell, Statoil, Total, Weatherford, Wintershall and Woodside Petroleum Limited. We are indebted to Jeffry Hamman, Maojin Tan, and two anonymous reviewers for their constructive technical and editorial comments that improved the first version of the manuscript.

Appendix A: Formulation of the Inverse Problem to Estimate a Bimodal Gaussian Pore-Size Distribution from MICP Data

The evaluation of a bimodal Gaussian pore-size distribution from MICP data is performed by minimizing the quadratic cost function:

$$C(x) = \left\| W_s \left[S_w(x) - S_{w,m} \right] \right\|_2^2 + \alpha^2 \|x\|_2^2, \tag{A.1}$$

where $S_w(x)$ is the modeled wetting-phase saturation that is equivalent to the CDF described in Eq. (2), $S_{w,m}$ is the measured wetting-phase saturation from MICP data,

W_s is a data-weighting matrix, α is a regulation (stabilization) parameter, and vector x contains the six Gaussian attributes, expressed as

$$x = [w_1, \log \mu_1, \log \sigma_1, w_2, \log \mu_2, \log \sigma_2]^T, \tag{A.2}$$

subject to

$$w_1 + w_2 = 1.0 \tag{A.3}$$

and

$$w_i > 0. \tag{A.4}$$

The superscript T in Eq. (A.2) indicates transpose.

Appendix B: Inverted Gaussian Attributes for 33 Core Samples with MICP

The inversion method was implemented to estimate bimodal Gaussian pore-size distributions from 33 MICP curves. Table 1 lists all Gaussian attributes together with total porosity, permeability, and irreducible water saturation (at $P_c = 1000$ psi) for each core sample.

Table 1 Gaussian attributes, total porosity, permeability, and irreducible water saturation for 33 core samples with MICP from the Hugoton Gas Field, Kansas

Sample No.	w_1 (frac)	w_2 (frac)	μ_1 (μm)	μ_2 (μm)	$\log \sigma_1$	$\log \sigma_2$	ϕ_t (frac)	k (mD)	S_{wirr} (frac)
1	0.680	0.320	2.230	0.209	0.098	0.713	0.187	15.681	0.112
2	0.554	0.446	1.079	0.092	0.019	0.682	0.098	0.376	0.233
3	0.372	0.628	3.304	0.303	0.206	0.626	0.156	5.728	0.154
4	0.562	0.439	8.025	0.545	0.173	0.954	0.125	29.712	0.116
5	0.657	0.343	0.495	0.077	0.299	0.792	0.076	0.110	0.201
6	0.360	0.640	1.500	0.080	0.500	0.050	0.134	0.774	0.671
7	0.650	0.350	2.993	0.651	0.175	0.551	0.237	28.284	0.044
8	0.538	0.462	0.677	0.134	0.213	0.486	0.142	0.774	0.196
9	0.652	0.348	0.182	0.055	0.137	1.307	0.111	0.246	0.275
10	0.585	0.415	2.933	0.402	0.158	0.856	0.188	19.771	0.109
11	0.308	0.692	2.016	0.292	0.247	0.797	0.189	13.885	0.217
12	0.710	0.290	3.184	0.694	0.101	0.885	0.194	30.500	0.056
13	0.722	0.278	3.243	0.512	0.078	1.048	0.224	65.302	0.070
14	0.794	0.207	3.244	0.353	0.071	1.199	0.261	102.711	0.066
15	0.998	0.002	0.052	0.024	0.767	0.011	0.131	0.010	0.648
16	0.629	0.371	0.310	0.094	0.199	0.724	0.095	0.031	0.217
17	0.868	0.132	0.220	0.069	0.498	3.397	0.048	0.002	0.300
18	0.565	0.435	2.416	0.343	0.194	0.753	0.160	5.850	0.099
19	0.483	0.518	1.261	0.300	0.112	0.549	0.157	1.951	0.109

Table 1 (*Continued*)

Sample No.	w_1 (frac)	w_2 (frac)	μ_1 (μm)	μ_2 (μm)	$\log \sigma_1$	$\log \sigma_2$	ϕ_t (frac)	k (mD)	S_{wirr} (frac)
20	0.353	0.648	1.479	0.216	0.158	0.750	0.093	0.428	0.220
21	0.513	0.487	1.589	0.230	0.133	0.757	0.123	1.537	0.155
22	0.758	0.242	0.366	0.027	0.297	0.889	0.089	0.048	0.228
23	0.568	0.433	0.410	0.059	0.351	0.801	0.129	0.357	0.308
24	0.683	0.317	0.295	0.045	0.207	0.703	0.123	0.065	0.254
25	0.497	0.503	0.667	0.223	0.154	0.428	0.161	0.496	0.109
26	0.372	0.628	0.441	0.055	0.144	0.612	0.122	0.061	0.426
27	0.947	0.053	0.029	0.011	0.139	0.016	0.096	0.002	1.000
28	0.533	0.467	0.614	0.011	0.170	1.113	0.103	0.136	0.371
29	0.574	0.426	0.779	0.061	0.213	0.519	0.127	0.553	0.287
30	0.123	0.877	0.022	0.011	0.165	0.029	0.035	0.001	1.000
31	0.550	0.450	0.059	0.048	0.622	0.213	0.072	0.009	0.843
32	0.710	0.291	0.102	0.028	0.163	0.724	0.076	0.014	0.690
33	0.430	0.570	0.406	0.125	0.046	0.490	0.061	0.023	0.266

References

Archie GE (1950) Introduction to petrophysics of reservoir rocks. Am Assoc Pet Geol Bull 34(5):943–961

Basan PB, Lowden BD, Whattler PR, Attard J (1997) Pore-size data in petrophysics: a perspective on the measurement of pore geometry. In: Geological Society Special Publications, vol 122, pp 47–67

Buiting JJM (2011) Upscaling saturation-height technology for Arab carbonates for improved transition-zone characterization. SPE Reserv Eval Eng 14(1):11–24

Burdine NT (1953) Relative permeability calculations from pore size distribution data. J Pet Technol 5(3):71–78

Childs EC, Collis-George N (1950) The permeability of porous materials. Proc R Soc A 201(1066):392–405

Clerke EA (2009) Permeability, relative permeability, microscopic displacement efficiency, and pore geometry of M_1 bimodal pore systems in Arab D limestone. SPE Journal 14(3):524–531

Clerke EA, Mueller HW, Phillips EC, Eyvazzadeh RY, Jones DH, Ramamoorthy R, Srivastava A (2008) Application of Thomeer hyperbolas to decode the pore systems, facies, and reservoir properties of the Upper Jurassic Arab D limestone, Ghawar field, Saudi Arabia: a "Rosetta Stone" approach. GeoArabia 13(4):113–160

Dubois MK, Byrnes AP, Bhattacharya S, Bohling GC, Doveton JH, Barba RE (2006) Hugoton Asset Management Project (HAMP). Hugoton Geomodel Final Report. KGS Open File Report

Gao B, Wu JH, Chen SH, Kwak H, Funk J (2011) New method for predicting capillary pressure curves from NMR data in carbonate rocks. In: SPWLA 52nd annual logging symposium, Colorado Springs, Colorado, May 14–18

Genty C, Jensen JL, Ahr WM (2007) Distinguishing carbonate reservoir pore facies with nuclear magnetic resonance measurements. Nat Resour Res 16(1):45–54

Handy LL, Datta P (1966) Fluid distributions during immiscible displacements in porous media. SPE Journal 6(3):261–266

Hidajat I, Mohanty KK, Flaum M, Hirasaki G (2004) Study of vuggy carbonates using X-ray CT scanner and NMR. SPE Reserv Eval Eng 7(5):365–377

Huang DD, Honarpour MM, Al-Hussainy R (1997) An improved model for relative permeability and capillary pressure incorporating wettability. In: Society of core analysts international symposium, Calgary, Canada, September 7–10

Marschall D, Gardner JS, Mardon D, Coates GR (1995) Method for correlating NMR relaxometry and mercury injection data. In: Society of core analysts international symposium, San Francisco, California, United States, September 7–10

Mohanty KK, Salter SJ (1982) Multiphase flow in porous media: II. pore-level modeling. In: SPE annual technical conference and exhibition, New Orleans, Louisiana, September 26–29

Nimmo JR (2004) Porosity and pore size distribution. In: Encyclopedia of soils in the environment, vol 3. Elsevier, London, pp 295–303

Olson TM, Babcock JA, Prasad KVK, Boughton SD, Wagner PD, Franklin MK, Thompson KA (1997) Reservoir characterization of the giant Hugoton gas field, Kansas. Am Assoc Pet Geol Bull 81(11):1785–1803

Peters EJ (2012) Advanced petrophysics—volumes 1 and 2. Greenleaf Book Group, Austin

Press WH, Teukolsky SA, Vetterling WT, Flannery BP (2007) Numerical recipes. the art of scientific computing, 3rd edn. Cambridge University Press, New York. Sect. 16.1: Gaussian mixture models and k-means clustering

Spencer DW (1963) The interpretation of grain size distribution curves of clastic sediments. J Sediment Res 33(1):180–190

Thomeer JHM (1960) Introduction of a pore geometrical factor defined by the capillary pressure curve. J Pet Technol 12(3):73–77

Xu C, Heidari Z, Torres-Verdín C (2012) Rock classification in carbonate reservoirs based on static and dynamic petrophysical properties estimated from conventional well logs. In: SPE annual technical conference and exhibition, San Antonio, Texas, October 5–9

Xu C, Torres-Verdín C (2012) Saturation-height and invasion consistent hydraulic rock typing using multi-well conventional logs. In: SPWLA 53rd annual logging symposium, Cartagena, Columbia, June 16–20

View publication stats